PHYSICAL REVIEW RESEARCH **5**, 033101 (2023)

Arbitrary nonequilibrium steady-state construction with a levitated nanoparticle

Yu Zheng, Lyu-Hang Liu, Xiang-Dong Chen, Guang-Can Guo, and Fang-Wen Sun[*]
CAS Key Lab of Quantum Information, University of Science and Technology of China, Hefei 230026, China
and CAS Center For Excellence in Quantum Information and Quantum Physics,
University of Science and Technology of China, Hefei 230026, China

(Received 3 November 2022; accepted 26 July 2023; published 14 August 2023)

Nonequilibrium thermodynamics provides a general framework for understanding nonequilibrium processes, particularly in small systems that are typically far from equilibrium and dominated by fluctuations. However, the experimental investigation of nonequilibrium thermodynamics remains challenging due to the lack of approaches to precisely manipulate nonequilibrium states and dynamics. Here, by shaping the effective potential of energy, we propose a general method to construct a nonequilibrium steady state (NESS) with arbitrary energy distribution. Using a well-designed energy-dependent feedback damping, the dynamics of an optically levitated nanoparticle in vacuum is manipulated and driven into a NESS with the desired energy distribution. Based on this approach, a phonon laser state is constructed with an ultra-narrow linewidth of 6.40 μHz. Such an arbitrary NESS construction method provides an approach to manipulating the dynamics processes of micromechanical systems and paves the way for the systematic study of nonequilibrium dynamics in interdisciplinary research fields.

DOI: 10.1103/PhysRevResearch.5.033101

I. INTRODUCTION

Originating from Maxwell's demon, a heat engine with feedback can break the second law of thermodynamics with the help of its microscopic state information [1,2]. Since the system can be controllably pushed away from equilibrium, it is ideally suitable for studying nonequilibrium dynamics. This is of importance not only in physics but also in the life and chemical sciences, where fluctuating systems far from equilibrium are a more common circumstance [3–5]. With extraordinary abilities to track and manipulate the dynamics of micro- and nanoparticles, optical tweezers have become a standard experimental platform for microscopic thermodynamic research. More recently, optical tweezers and levitation in vacuum have shown excellent performance in demonstrations of fundamental physics [6–8], macroscopic quantum mechanics [9–11], precision measurements [12–16], and in particular, microscopic thermodynamics [17–23]. The ability to create a NESS and manipulate the strength of environmental interactions makes it appropriate for detailed studies of nonequilibrium thermodynamics under the influence of fluctuations [6,21].

However, existing nonequilibrium experimental preparations are "scheme-to-state" approaches that rely on particular feedback control schemes to generate specific NESSs that correspond to the schemes [18,24]. A general design principle starting from any desired state remains to be investigated. Here we introduce a universal approach based on the shaping of the energy effective potential [22] that allows the construction of an arbitrary NESS with the help of energy-dependent feedback damping. A variety of NESSs, including the phonon laser state, can be constructed using this approach. These customized motion states can be used for the investigation of nonequilibrium thermodynamics and precision measurements. Moreover, this prototype scheme can be further developed for manipulating levitated macroscopic quantum states [9–11].

II. ARBITRARY NESS CONSTRUCTION

A. Construction principle

Considering an optically levitated nanoparticle in vacuum with an air damping Γ_0. Without any external interaction, the steady state of the nanoparticle will be a thermodynamic equilibrium state. To obtain a NESS, extra channels for the exchange of energy or material are necessary. A damping rate Γ_m is used to describe the rate and direction of energy exchange. Here, we deploy an energy-dependent damping $\Gamma_m(E)$ to try to drive the system into a NESS. In this case, the particle's energy dynamics can be manifested as a Markovian stochastic process. Its energy dynamics are similar to an overdamped Brownian motion. The stochastic dynamic of a levitated nanoparticle's mechanical energy E can be described with a Langevin equation [18] (see also Appendix A for more details), and we can obtain the energy effective potential, which is

$$U(E) = \frac{1}{\Gamma_0}\int [\Gamma_m(E) + \Gamma_0] dE. \quad (1)$$

---

[*] fwsun@ustc.edu.cn

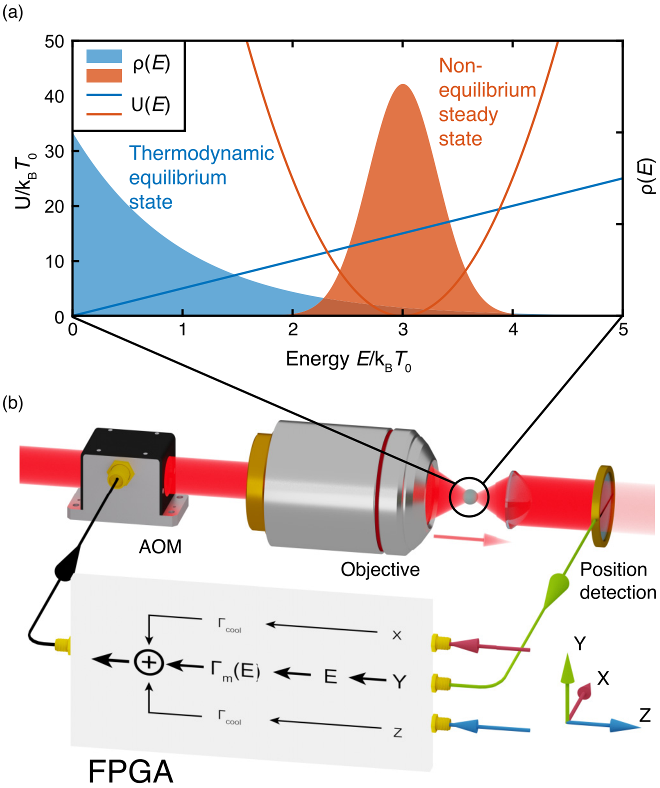

FIG. 1. Schematic diagram of the construction of arbitrary NESSs. (a) Modification of the energy effective potential $U(E)$ (solid lines) will change the corresponding energy distribution $\rho(E)$ (colored areas). (b) Experimental configuration. The energy distribution of a silica nanoparticle (radius ∼ 75 nm) trapped by a tightly focused laser beam is modified by the feedback control damping [$\Gamma_m(E)$], which is based on the real-time measurement of the translational degrees of freedom of the nanoparticle.

Therefore the distribution of E corresponding to Eq. (1) can be given as a Boltzmann distribution [18,22],

$$\rho(E) = \frac{1}{Z}\exp\left[-\beta_0 U(E)\right], \tag{2}$$

where $Z = \int_0^\infty \exp[-\beta_0 U(E)]\mathrm{d}E$, $\beta_0 = 1/k_B T_0$, where k_B is the Boltzmann constant, and T_0 is the particle's center-of-mass motion temperature under thermodynamic equilibrium.

From Eq. (2) we are able to manipulate the feedback damping as

$$\Gamma_m(E) = -\frac{\Gamma_0}{\beta_0}\frac{1}{\rho(E)}\frac{d\rho(E)}{dE} - \Gamma_0, \tag{3}$$

and create a specific NESS with energy distribution $\rho(E)$ by deploying this $\Gamma_m(E)$ to the system.

B. NESS construction results

In the experiment we verify the feasibility of the construction of an arbitrary NESS of a levitated nanoparticle. As shown in Fig. 1(b), a silica nanosphere with a diameter of approximately 150 nm is trapped in vacuum by an optical potential with a tightly focused, linearly polarized, 1064-nm laser. We monitor the particle's real-time position and obtain its energy E with a custom-programmed field-programmable gate array (FPGA) board. The energy-dependent damping $\Gamma_m(E)$ can be added to the system by modulating the trapping laser power through the parametric feedback control protocol [25–27]. By controlling the depth and phase of the parametric feedback control signal, it is able to generate the energy-dependent feedback damping rate in an achievable range [26,27]. Therefore it is possible to obtain the desired $\rho(E)$ by deploying the designed $\Gamma_m(E)$ (see Appendix B for details).

Figure 2 shows the NESS construction results with three different $\Gamma_m(E)$. Moreover, a thermal equilibrium state with $\Gamma_m = 0$ is shown in Fig. 2(a) as a comparison.

As shown in Fig. 2(b), $\Gamma_m(E)$ with a step function can be used to lock the oscillation amplitude of the levitated nanoparticle, which has been applied in a high-accuracy position and mass measurement [26]. When the energy of the oscillator is lower (higher) than the target energy, a fixed negative (positive) feedback damping is applied to increase (decrease) the energy of the oscillator. Such a two-stage step function creates a V-type $U(E)$, corresponding to a wedge shape $\rho(E)$.

We can construct an interesting NESS with a flat-top energy distribution, which can be used in the simulation of a free Brownian particle's diffusion process. From Eq. (3), a continuous uniform distribution of energy, which means $d\rho(E)/dE = 0$, requires $\Gamma_m(E) = -\Gamma_0$. In other words, feedback damping is required to accurately offset the air damping to create the flat top. To fulfill the requirement, a $-\Gamma_0$ part is inserted into a step function $\Gamma_m(E)$, as shown in Fig. 2(c). It can be observed that the oscillator's energy distribution is almost uniform in the $-\Gamma_0$ part. The slight fluctuation is caused by the vacuum pressure drift during data collection.

Finally, we attempt to make a double-well potential in energy, which is significant in bistable state studies such as Kramers turnover [6] or Landauer's principle [28]. Similar to the potential well structure in space, according to Eq. (1) it is feasible to construct a double well $U(E)$ with a cubic function $\Gamma_m(E)$, as shown in Fig. 2(d). Because the maximum achievable feedback damping rate in our system is ±2000 Hz, parts of $\Gamma_m(E)$ that exceed the limitation are truncated. The experimental result shows that the oscillator has a twin-peak energy distribution, and its phase plot has a double-ring pattern. Incidentally, the cubic function $\Gamma_m(E)$ used in double-well potential construction is compensated with a $-\Gamma_0$. Otherwise, the energy distribution will be asymmetric.

III. PHONON LASER CONSTRUCTION

A. Principle of phonon laser construction

Moreover, the phonon laser is one of the most important NESS states, which can be utilized as a coherent phonon source or as an ultrasensitive sensor [24,29–32]. Based on this NESS construction platform, we can concisely create a phonon laser state by a well-designed $U(E)$, which corresponds to $U(N)$ with $N = E/\hbar\Omega_0$, where N is the phonon number and Ω_0 is the eigenfrequency of the oscillator. The phonon number distribution of the phonon laser that is well above the threshold will show a Gaussian distribution, which corresponds to a quadratic $U(N)$. Therefore, according to Eq. (1), a phonon laser can be constructed by deploying a

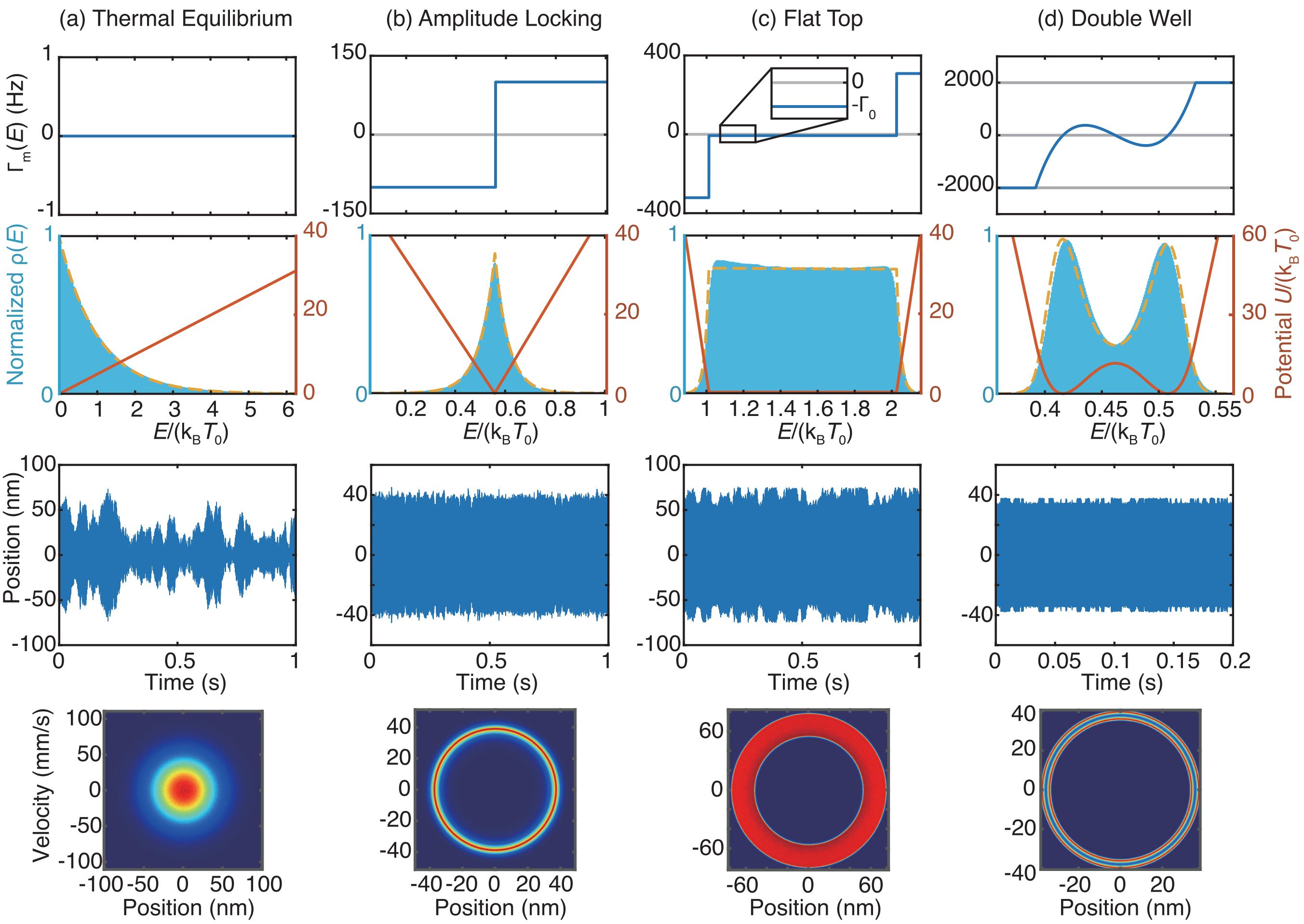

FIG. 2. Experiment result of NESS construction under different $\Gamma_m(E)$. (a) Thermal equilibrium state as a comparison. (b)–(d) Three types of NESS constructions result, which is amplitude locking state by a step function $\Gamma_m(E)$, flat-top distributed state, and double-well state. (1st row) $\Gamma_m(E)$ deployed for the construction of each state. (2nd row) Energy effective potential $U(E)$ and the measurement energy distribution $\rho(E)$ under $\Gamma_m(E)$ from each state. The solid lines are $U(E)$ according to Eq. (1). The dashed lines are the theoretical expectations of the energy distribution according to Eq. (2). (3rd row) Part of the trajectories of each state. (4th row) Phase plots of the measured oscillator's motion from each state. The air pressure is 10^{-3} mbar during the data collection. The recording duration is 500 s for (a), (c) and 50 s for (b), (d).

linear function $\Gamma_m(N)$ to the nano-oscillator [24], that is

$$\Gamma_m(N) = \gamma_c N - \gamma_a, \tag{4}$$

where γ_a is the linear gain factor and γ_c is the nonlinear cooling factor. The dynamical equation of the phonon number can be written as (see Appendix C for details)

$$\dot{N} = (\gamma_a - \Gamma_0)N - \gamma_c N^2 + \frac{\Gamma_0 k_B T_0}{\hbar\Omega_0} + A, \tag{5}$$

where $A = \sqrt{2N\Gamma_0 k_B T_0/\hbar\Omega_0}dW/dt$ is the stochastic part and W is the Wiener process.

According to Eq. (2), the phonon number distribution fulfills

$$\rho(N) = \frac{1}{Z_N}\exp\left\{-\beta_0\left(\frac{\hbar\Omega_0\gamma_c}{2\Gamma_0}\left[N - \frac{(\gamma_a - \Gamma_0)}{\gamma_c}\right]^2\right)\right\}, \tag{6}$$

where Z_N is the normalization factor. Equation (6) is a Gaussian distribution function which has a mean value of

$$\langle N\rangle = (\gamma_a - \Gamma_0)/\gamma_c \tag{7}$$

and variance of

$$\mathrm{Var}(N) = \frac{\hbar\Omega_0\gamma_c}{k_B T_0 \Gamma_0}. \tag{8}$$

It should be mentioned that since the phonon number N can only be positive, the actual phonon number distribution $\rho(N)$ is only the positive half-axis part from Eq. (6).

B. Experiment result

In the experiment we construct different $\Gamma_m(N)$ to obtain phonon lasers with various phonon number distributions. During the experiment we keep γ_c constant and increase the value of γ_a, as shown in Fig. 3(a). It can be see from Fig. 3(b) that the mean phonon number of the oscillator is increased with the increasing γ_a. Meanwhile, the shape of the phonon number distribution $\rho(N)$ remains the same. Such an experimental result can also be obtained from Eqs. (7) and (8), that the $\langle N\rangle$ increases linearly with γ_a and $\mathrm{Var}(N)$ is only related with γ_c.

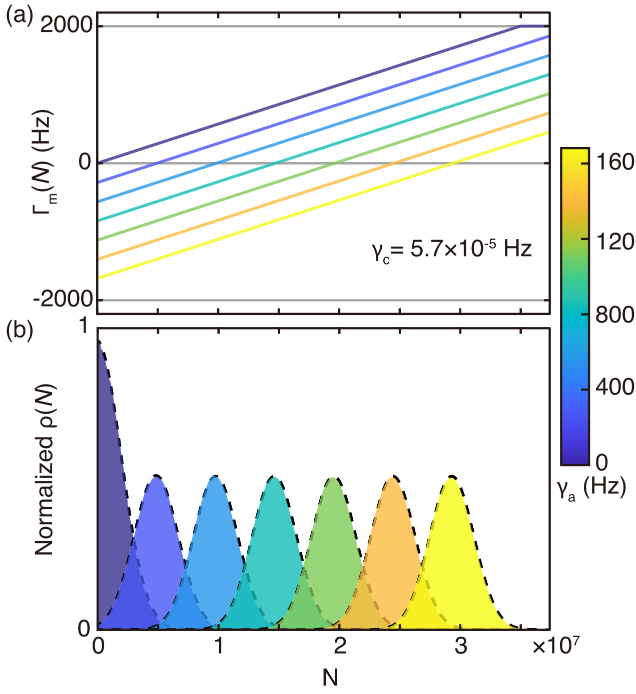

FIG. 3. Experiment result of phonon laser construction. (a) The phonon-dependent feedback damping $\Gamma_\mathrm{m}(N)$ with a fixed γ_c and an increasing γ_a that is deployed on the trapped nanoparticle. (b) The measured phonon number distribution of the nanoparticle driven by $\Gamma_\mathrm{m}(N)$ from (a). The dashed lines are the theoretical expectations according to Eq. (6). In these figures, γ_c is a constant with $\gamma_c = 5.7 \times 10^{-5}$ Hz, and the pressure is 10^{-3} mbar.

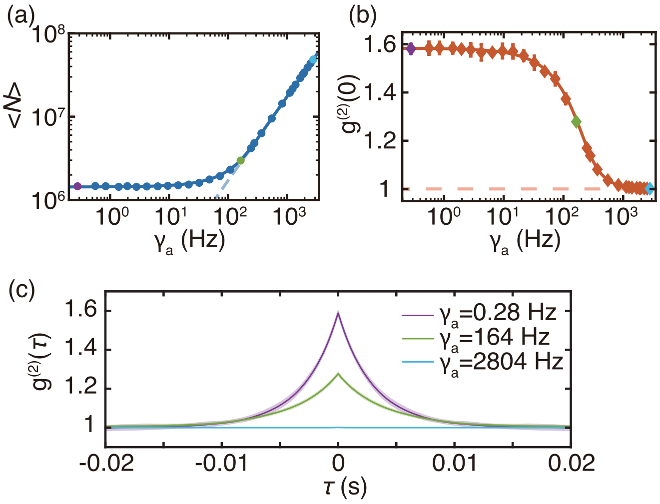

FIG. 4. Coherence result of phonon laser. (a) Mean phonon number $\langle N\rangle$ as a function of the gain factor γ_a. The dashed line follows Eq. (7). The error bars are smaller than the data mark. (b) Second-order phonon autocorrelation function at zero delay, $g^{(2)}(0)$, as a function of the gain factor γ_a. The solid lines in (a) and (b) are theoretical expectations based on Eq. (6). (c) $g^{(2)}(\tau)$ with different γ_a. the selected point is marked with the same color in (a) and (b). The error is marked with the color areas. The standard deviation represented by error bars or areas in (a), (b), and (c) is calculated from ten measurements. In these figures, γ_c is a constant with $\gamma_c = 5.7 \times 10^{-5}$ Hz, and the pressure is 10^{-3} mbar.

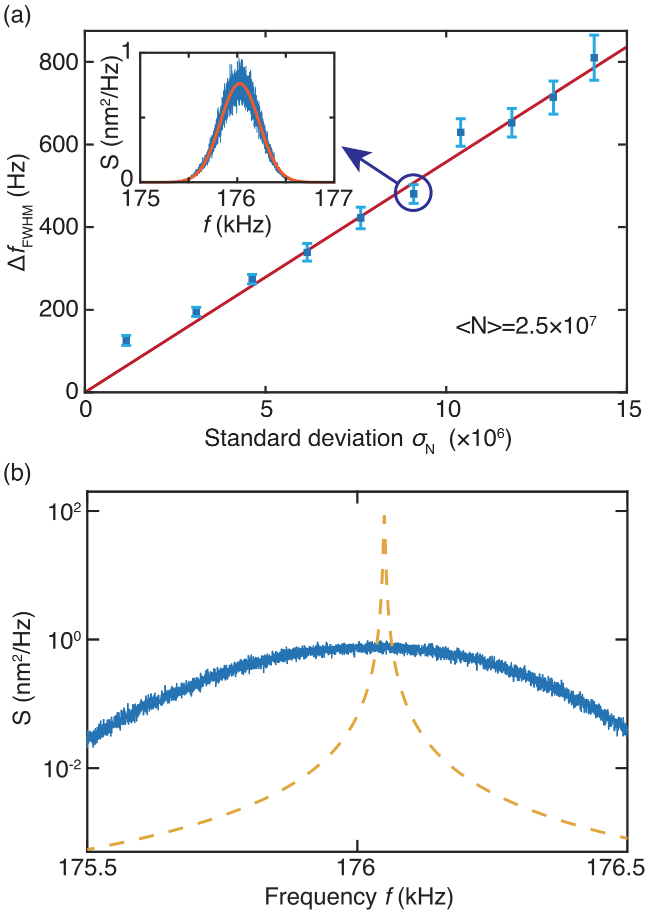

FIG. 5. Experimental verification of nonlinearity widening. (a) Δf_FWHM as a function of σ_N. $\langle N\rangle$ remains constant during the experiment. The solid line is a fitting of Eq. (D19). Error bars represent the s.d. that are calculated from ten measurements of a 5-s trajectory. The inset figure is the PSD of the selected data point. The orange line in the inset is a fitting of the Gaussian function. (b) Comparing the measured PSD (solid line) with the theoretical PSD (dash line) of a harmonic free-run phonon laser. The measured PSD is from the insert figure in (a). The theoretical PSD is calculated from Eq. (D13) with the experimental conditions.

To study the phonon laser threshold and coherence properties, the linear gain factor γ_a is selected as the pump power coefficient. The threshold property of a laser is verified by increasing γ_a from 0 Hz. Figure 4(a) shows that when γ_a exceeds a threshold, the mean phonon number $\langle N\rangle$ increases linearly with γ_a. As shown in Figs. 4(b) and 4(c), as γ_a increases from zero to well above the threshold, $g^{(2)}(0)$ decreases to 1, which means that the oscillation changes from a thermal state to a coherent state. It can be noticed that $g^{(2)}(0)$ does not start from 2 when $\gamma_a = 0$ Hz. This is because the nonlinear cooling factor γ_c is a nonzero constant, which compels the system to deviate from a pure thermal state.

C. Linewidth of phonon laser

The narrowing of linewidth is another important feature of lasers [24,30]. Utilizing the analysis of the stochastic phase noise, the full width at half maximum linewidth of a free-run

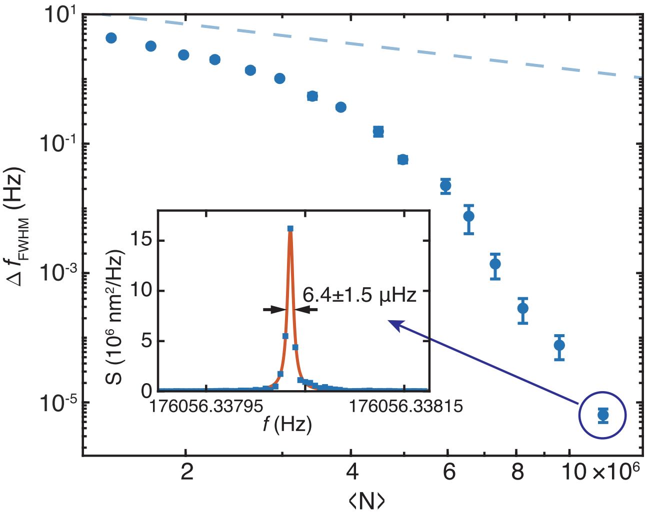

FIG. 6. PSD linewidth $\Delta f_{\rm FWHM}$ of phonon laser state as a function of the mean phonon number with feedback frequency stabilization. Error bars represent the standard deviations that are calculated from five trajectories of each data point. The recording time of each sampling data point ranges from 200 to 2×10^5 s depending on the linewidth required spectrum resolution. The dashed line is the theoretical linewidth of a free-run phonon laser from Eq. (9). The inset figure is the averaged PSD of the selected data point trajectories. The solid line in the inset is a fitting of the Lorentzian function. The data are recorded at a pressure of 10^{-3} mbar. The corresponding phonon laser parameters are $\gamma_c = 5 \times 10^{-5}$ Hz and $\gamma_a = 20$ to 600 Hz.

phonon laser is supposed to be

$$\Delta f_{\rm FWHM} = \frac{k_{\rm B} T_0 \Gamma_0}{4\pi \langle N \rangle \hbar \Omega_0}. \tag{9}$$

And the shape of the free-run phonon laser's power spectral density (PSD) would be a Lorentzian function (see Appendix D1 for details).

However, the presence of the Duffing nonlinearity in the optical potential [33–35] causes the oscillator's frequency to depend on its amplitude. Consequently, the dispersion of the phonon number results in a frequency shift that significantly broadens the linewidth beyond the theoretical value of a free-run phonon laser. The experimental verification of the Duffing nonlinearity-induced width is shown in Fig. 5. That is, $\Delta f_{\rm FWHM}$ is proportional to the standard deviation of phonon number $\sigma_N = \sqrt{{\rm Var}(N)}$, and the PSD can be fitted with a Gaussian function, as the phonon number distribution is also a Gaussian function (see Appendix D2 for details). A narrower phonon number distribution can mitigate nonlinearity-induced spectrum widening. However, due to the limitation of control precision, it is difficult to approach the linewidth of a free-run phonon laser.

To overcome this challenge, an active feedback frequency stabilization based on an integral feedback controller is deployed. The duration of each oscillation cycle is compared with the period corresponding to the locking frequency. The frequency error is compensated by modulating the base intensity of the trapping laser. As shown in Fig. 6, under frequency stabilization, the linewidth of the phonon laser decreases when the mean phonon number increases. The measured phonon laser linewidth is much narrower than the theoretical free-run linewidth, which indicates that the phase noise error introduced by the stochastic and nonlinear process in the phonon laser is well suppressed by the frequency stabilization. The narrowest linewidth recorded in the experiment is $\Delta f_{\rm FWHM} = 6.40(\pm 1.51)$ μHz, and the corresponding coherent time is $T_{\rm C} = 46 \pm 11$ h, which can be further applied in the precision measurement requiring long-term stabilization like ultraweak gravity force detection [36].

IV. CONCLUSION

In conclusion, we have introduced an energy-dependent feedback damping to construct a NESS with an arbitrary energy distribution of an optically levitated nanoparticle. The feasibility of this method has been experimentally verified by demonstrating special steady states that have never been reported. Moreover, a phonon laser steady state with an ultranarrow linewidth is produced by this method.

The energy flow control and state manipulation shown in this work could be used to reinforce optical levitation as an excellent platform for microscopic thermodynamic investigation, including nonequilibrium, stochastic, and information thermodynamics. The NESS construction makes it possible for the experimental verification of advanced thermodynamic ideas such as the finite-time Landauer principle [37], the Brownian motor [38,39], and the Mpemba effect [40,41]. Moreover, the NESS construction in here can be applied to any nano-, micromechanical system that can be feedback controlled. Compared with the conventional nonlinearity-based phonon laser, the phonon laser generation here has less limitation on the properties such as mean phonon number, which makes it possible to generate a low-phonon-number coherent state, such as a phonon Fock state. The stabilized phonon lasers can benefit the development of precision measurements based on levitated nanosensors [42], such as ultraweak force detection.

ACKNOWLEDGMENTS

We acknowledge support from the National Natural Science Foundation of China (Grants No. 12104438 and No. 62225506), CAS Project for Young Scientists in Basic Research (Grant No. YSBR-049), and the Fundamental Research Funds for the Central Universities. The sample preparation was partially conducted at the USTC Center for Micro and Nanoscale Research and Fabrication.

APPENDIX A: DERIVATION OF $U(E)$ AND $\rho(E)$ UNDER $\Gamma_{\rm m}(E)$

This section shows the deviation of $\rho(E)$ and $U(E)$ in the main text from a levitated nanoparticle's equation of motion. The derivation process generally refers to the process in Ref. [18].

Following the steps in Ref. [18], the motion of a trapped nanoparticle in an independent motion dimension is considered. The equation of motion can be written as

$$\ddot{q}(t) + [\Gamma_0 + \Gamma_\mathrm{m}(t)]\dot{q}(t) + \Omega_0^2 q(t) = \frac{1}{m} F_\mathrm{random}(t), \tag{A1}$$

where q is the position of the particle, Γ_0 is the air damping rate, $\Gamma_\mathrm{m}[E(t)]$ is the feedback damping rate, Ω_0 is the eigenfrequency of the particle's oscillation, m is the particle's mass, $F_\mathrm{random}(t) = \sqrt{2m\Gamma_0 k_\mathrm{B} T_0}\,\xi(t)$ is the stochastic force from the environment (air molecule collisions), T_0 is the center-of-mass (COM) temperature, and $\xi(t) = dW(t)/dt$, where W is the Wiener process.

Rewriting Eq. (A1) into a stochastic differential equation (SDE), we have

$$dq = \frac{p}{m} dt, \tag{A2}$$

$$dp = \left[-m\Omega_0^2 q - \Gamma_0 p - \Gamma_\mathrm{m}(t)p\right]dt + \sqrt{2m\Gamma_0 k_\mathrm{B} T_0}\, dW, \tag{A3}$$

where p is the particle's momentum.

Consider the dynamics in the particle's energy E. To avoid multiplicative noise, the dynamics of energy are described in ϵ such that $\epsilon = \sqrt{E}$. Neglecting all terms that higher the order of $(dt)^{3/2}$, we have

$$d\epsilon = \left(\frac{\partial \epsilon}{\partial q}\right) dq + \left(\frac{\partial \epsilon}{\partial p}\right) dp + \frac{1}{2}\left(\frac{\partial^2 \epsilon}{\partial p^2}\right)(dp)^2. \tag{A4}$$

With

$$E(q, p) = \frac{1}{2} m\Omega_0^2 q^2 + \frac{p^2}{2m} \tag{A5}$$

and Eqs. (A2) and (A3), Eq. (A4) can be obtained as

$$\begin{aligned} d\epsilon &= m\Omega_0^2 \frac{q}{2\epsilon} dq + \frac{1}{2\epsilon}\frac{p}{m} dp + \frac{1}{2}\left(\frac{1}{2m\epsilon} - \frac{1}{4\epsilon^3}\frac{p^2}{m^2}\right)(dp)^2 \\ &= \frac{1}{2\epsilon}\frac{p^2}{m}[-\Gamma_0 + \Gamma_\mathrm{m}(\epsilon)]dt + \frac{1}{2\epsilon}\frac{p}{m}\sqrt{2m\Gamma_0 k_B T_0}\, dW \\ &\quad + \frac{1}{2\epsilon}\left(1 - \frac{p^2}{2m\epsilon^2}\right)\Gamma_0 k_B T_0 (dW)^2. \end{aligned} \tag{A6}$$

Next we use quasistatic approximations. The coherence time of the levitated oscillator in high vacuum is much longer than its oscillation period. In one period the energy can be considered as a constant, and the velocity can be approximated as a sine function. We focus on the energy varying in one oscillation period, $\tau = 2\pi/\Omega_0$, which is

$$\begin{aligned} \Delta\epsilon = \int_0^\tau d\epsilon &= -\frac{\Gamma_0}{2}\int_0^\tau \frac{p^2}{m\epsilon} dt - \frac{1}{2}\int_0^\tau \frac{\Gamma_\mathrm{m}(\epsilon)p^2}{m\epsilon} dt \\ &\quad + \sqrt{2m\Gamma_0 k_\mathrm{B} T_0}\int_0^\tau \frac{p}{2m\epsilon} dW \\ &\quad + \Gamma_0 k_\mathrm{B} T_0 \int_0^\tau \frac{1}{2\epsilon}\left(1 - \frac{p^2}{2m\epsilon^2}\right)(dW)^2, \end{aligned} \tag{A7}$$

and we have [18]

$$\Delta\epsilon = \left(-\frac{(\Gamma_0 + \Gamma_\mathrm{m})\epsilon}{2} + \frac{\Gamma_0 k_\mathrm{B} T_0}{4\epsilon}\right)\tau + \sqrt{\frac{\Gamma_0 k_\mathrm{B} T_0}{2}}\, W(\tau). \tag{A8}$$

Rewriting Eq. (A8) into a differentiated form, we have

$$d\epsilon = \frac{1}{\nu} f(\epsilon) dt + \sqrt{\frac{2k_\mathrm{B} T_0}{\nu}}\, dW, \tag{A9}$$

where $\nu = 4/\Gamma_0$ and

$$f(\epsilon) = -2\epsilon\left(\frac{\Gamma_0 + \Gamma_\mathrm{m}(\epsilon)}{\Gamma_0}\right) + \frac{k_\mathrm{B} T_0}{\epsilon}. \tag{A10}$$

Equation (A9) is a Langevin equation. We can obtain the energy properties of the nanoparticle from the general properties of a Langevin equation.

The energy effective potential is

$$\begin{aligned} U_\epsilon(\epsilon) &= -\int f(\epsilon) d\epsilon \\ &= \epsilon^2 + \frac{2}{\Gamma_0}\int \epsilon\Gamma_\mathrm{m}(\epsilon) d\epsilon - k_\mathrm{B} T_0 \ln \epsilon. \end{aligned} \tag{A11}$$

The energy distribution follows the Maxwell-Boltzmann distribution, which is

$$\begin{aligned} \rho(\epsilon) &= \frac{1}{Z_\epsilon} \exp\left[-\beta_0 U_\epsilon(\epsilon)\right] \\ &= \frac{1}{Z_\epsilon}\epsilon \exp\left\{-\beta_0\left(\epsilon^2 + \frac{2}{\Gamma_0}\int \epsilon\Gamma_\mathrm{m}(\epsilon) d\epsilon\right)\right\}, \end{aligned} \tag{A12}$$

where $\beta_0 = 1/(k_\mathrm{B} T_0)$, Z_ϵ is the partition function.

Change the variable in the distribution Eq. (A12) from ϵ to E. We have Eq. (2) in the main text, that is,

$$\rho(E) = \frac{1}{Z} \exp\left\{-\frac{\beta_0}{\Gamma_0}\int [\Gamma_\mathrm{m}(E) + \Gamma_0] dE\right\}. \tag{A13}$$

Imitate the relation that $\rho(\epsilon) = \frac{1}{Z_\epsilon}\exp[-\beta_0 U_\epsilon(\epsilon)]$. We can have the effective potential for the energy that is

$$U(E) = \frac{1}{\Gamma_0}\int [\Gamma_\mathrm{m}(E) + \Gamma_0] dE, \tag{A14}$$

which is also Eq. (1) in the main text.

We should note that $U(E)$ can be utilized to obtain the statistical properties of energy E, such as the distribution or mean value. However, the dynamic properties such as diffusion are better to be investigated using ϵ and $U_\epsilon(\epsilon)$, as the Langevin equation Eq. (A9) can only be obtained with variable ϵ.

APPENDIX B: EXPERIMENTAL SETUP

The detailed schematic of the experiment setup is shown in Fig. 7.

1. Device structure

A CW 1064-nm laser (Coherent Mephisto 2000) is used as the trapping laser. Its intensity is modulated by an acousticoptic modulator (AOM). After the beam expand lens set, the laser beam with a diameter of approximately 4.5 mm is guided into an objective (N.A. = 0.9, Nikon CFI LU Plan Fluor EPI 100X) inside a vacuum chamber. The laser intensity before the objective is measured to be 250 mW. The trapping laser is focused by the objective to form the optical potential for particle trapping. After the objective, an aspheric lens (N.A. = 0.55, Thorlabs C230TME-1064) collects the forward

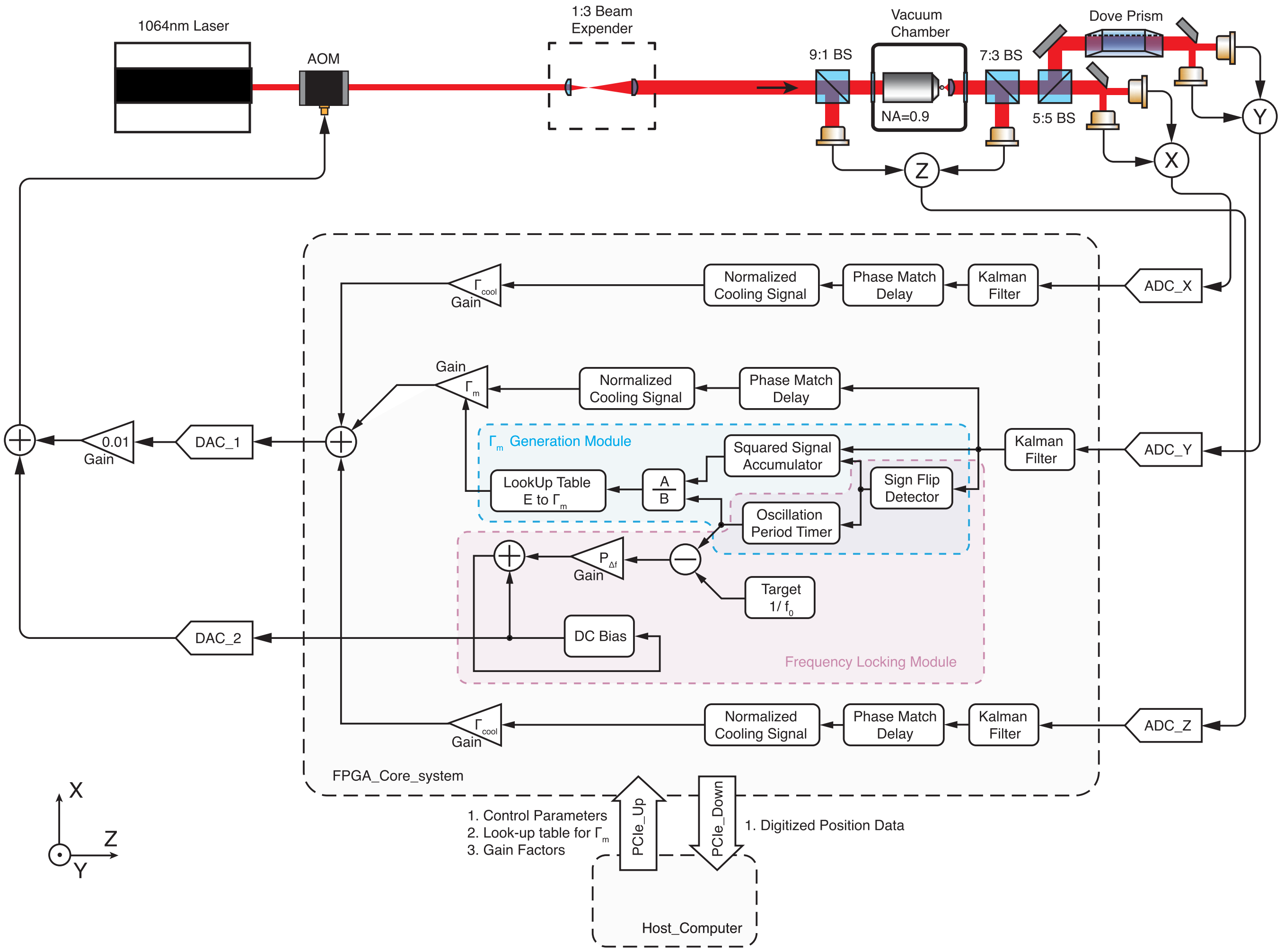

FIG. 7. Experimental configuration illustration.

scattering light and sends it to the particle position detection unit, which consists of three sets of homemade balanced photodetectors, to monitor the trapped particle's three motional degrees (set as X, Y, Z-axis) of freedom. A Dove prism is used to rotate the forward scattering light by 90° for the convention of Y-axis motion detection. The position signals are sent to a field-programmable gate array (FPGA) board to generate the feedback signal.

2. FPGA program structure

The position voltage signals from balanced photodetectors are processed by an FMC card, which has four channels of 16-bit ADC and two channels of 14-bit DAC. The digitized position signals are transferred to the FPGA core (Xilinx Virtex UltraScale+ XCVU3P) to generate the feedback control signal.

We focus on the nonequilibrium steady state (NESS) control signal generation of Y-axis motion. First, the position signal is processed by a Kalman filter to eliminate the out-band noise. Then the signal is sent to three modules. One is used to generate a normalized cooling signal. One is used to calculate the energy of the oscillator for Γ_m generation. And the last one is used to lock the oscillator's frequency. The details of cooling signal generation are described in Ref. [27].

Next we discuss the process of Γ_m generation. As the energy of a harmonic oscillator is proportional to the square of the amplitude, the energy calculation is accomplished by averaging the square of the position displacement of every data point in one oscillation cycle. A "sign flip detector" monitors the timing when the position signal's sign flips from negative to positive. When the sign flip event occurs, the "sign flip detector" sends a trigger signal to refresh the output data of the "squared signal accumulator" and the "oscillation period timer" and clear the two modules' counter. The output data of the two modules are divided to obtain the variable that is proportional to the energy.

Then the calculated energy E is sent to a lookup table. The map of $\Gamma_\mathrm{m}(E)$ is stored in the lookup table. We can obtain the feedback damping $\Gamma_\mathrm{m}(E)$ that corresponds to the measured E. $\Gamma_\mathrm{m}(E)$ multiplies the normalized cooling signal, and the parametric feedback control signal of the NESS is prepared finally.

However, this energy calculation introduces an additional feedback delay time of one oscillation period. In most situations the slow variation of the particle's energy in vacuum eliminates the effects of energy calculation delay. However, if the energy variation is too fast, the energy calculation delay's influence is observable. For example, the slight mismatch between the theoretical energy distribution and the measured distribution in Fig. 2(d) in the main text is because the feedback control cannot perfectly catch up with the switching events that the particle jumps between the two wells as the energy dramatically changes during well switching.

The NESS control signal is added with the cooling signals of the x and z axis and output through a DAC channel. The amplitude of the DAC output signal is reduced by 100 times with an amplifier to increase the control precision of the feedback damping. The output signal is added up with a dc bias voltage, which makes the AOM work in the linear regime and is sent to the rf driver of the AOM.

The motion of the x and z axis is cooled to about 10 K to minimize nonlinear coupling between different axes. It should be noted that the COM motion temperature of the above two axes should not be cooled too low; otherwise, the y-axis signal with higher amplitude will sneak into the feedback cooling loop of the x and z axis due to the cross-talk of position signals. This will introduce an unexpected cooling damping to the y-axis motion, thereby undermining the accuracy of the feedback damping $\Gamma_{\mathrm{m}}(E)$ applied to the y-axis motion.

The feedback frequency stabilization of a phonon laser is achieved by modulating the dc bias. As the oscillator's frequency is proportional to the square root of the laser intensity, the oscillator's frequency can be modulated by adjusting the dc bias of the AOM.

A simple integral controller is utilized to lock the oscillation frequency. The output of the "oscillation period timer" is compared with the target period. The difference is multiplied by a gain factor and added to the current dc bias. The addition result is looped back to the dc bias variable and becomes the new dc bias. The refresh loop of the dc bias is also triggered by the "sign flip detector."

The position signal processed in the FPGA is also transferred to a computer for data processing. Therefore, the ADC for data collection and the FPGA modules are driven by the same clock, which is necessary for ultra-narrow-linewidth phonon laser experiments.

3. Data processing for the energy and phase plot

The particle's position can be obtained from the calibrated photodetector signal. To obtain the particle's energy and phase plot, we also need to get the velocity of the particle. To obtain the velocity, we use the finite-difference method.

The detailed process is shown as follows. First, the raw position data is processed with a bandpass filter to eliminate out-band noise. And we have the position data x_i with $i = 1 \sim N$, and the sampling interval of the position data is Δt. Then a cubic spline interpolation is used to double the sampling rate, so that $x'_{2i-1} = x_i$ is the measured position data and x'_{2i} is the interpolated position data. And we have

$$v'_{j-1} = \frac{x'_{2j} - x'_{2(j-1)}}{\Delta t}, \tag{B1}$$

with $j = 2 \sim N$.

v'_{j-1} is smaller than the true velocity due to the truncation error in the finite-difference approximation. To compensate this error, v'_{j-1} has to be multiplied by a factor c. For a sine function with frequency f_0, we have

$$c = \frac{\pi f_0 \Delta t}{\sin(\pi f_0 \Delta t)}. \tag{B2}$$

The particle's velocity is $v_{j-1} = c v'_{j-1}$, where the particle's eigenfrequency is used to be f_0 for the calculation of c.

The phase trajectory of the particle is (x_j, v_{j-1}). The phase plot is the distribution of the phase trajectory on the phase plane. The purpose of using interpolated data to calculate the velocity is to make the velocity samples match the phase of the position samples. Otherwise, the obtained phase plot would be skewed.

The particle's energy can be calculated with

$$E_{j-1} = \tfrac{1}{2} m v_{j-1}^2 + \tfrac{1}{2} m \Omega_0^2 x_j^2, \tag{B3}$$

where m is the mass of the particle, and Ω_0 is the eigen angular frequency of the particle's oscillation.

APPENDIX C: DERIVATION OF THE PHONON LASER'S DYNAMICAL EQUATION

This section shows the deviation of the phonon laser's dynamical equation, which is Eq. (5) in the main text. We now rewrite Eq. (A9) into

$$d\epsilon = \mu dt + \sigma dW, \tag{C1}$$

where $\mu = -\epsilon[\Gamma_0 + \Gamma_{\mathrm{m}}(\epsilon)]/2 + \Gamma_0 k_{\mathrm{B}} T_0 / 4\epsilon$, and $\sigma = \sqrt{\Gamma_0 k_{\mathrm{B}} T_0 / 2}$.

According to its lemma and $E = \epsilon^2$, we have

$$\begin{aligned} E &= \left(\mu \frac{\partial E}{\partial \epsilon} + \frac{\sigma^2}{2} \frac{\partial^2 E}{\partial \epsilon^2} \right) dt + \sigma \frac{\partial E}{\partial \epsilon} dW \\ &= (2\epsilon\mu + \sigma^2) dt + 2\sigma\epsilon dW \\ &= (-E[\Gamma_0 + \Gamma_{\mathrm{m}}(E)] + \Gamma_0 k_{\mathrm{B}} T_0) dt + \sqrt{2E\Gamma_0 k_{\mathrm{B}} T_0} dW. \end{aligned} \tag{C2}$$

Replace energy E with phonon number $(N)\hbar\Omega_0$ and set the feedback damping Γ_{m} to the phonon laser control damping, which is $\Gamma_{\mathrm{m}}(N) = \gamma_c N - \gamma_a$. Equation (C2) can be written as

$$dN = (-N[\Gamma_0 + \Gamma_{\mathrm{m}}(N)] + \frac{\Gamma_0 k_{\mathrm{B}} T_0}{\hbar\Omega_0}) dt + \sqrt{\frac{2N\Gamma_0 k_{\mathrm{B}} T_0}{\hbar\Omega_0}} dW. \tag{C3}$$

We have the phonon laser's dynamical equation, which is

$$\dot{N} = (\gamma_a - \Gamma_0) N - \gamma_c N^2 + \frac{\Gamma_0 k_{\mathrm{B}} T_0}{\hbar\Omega_0} + \sqrt{\frac{2N\Gamma_0 k_{\mathrm{B}} T_0}{\hbar\Omega_0}} \frac{dW}{dt}. \tag{C4}$$

APPENDIX D: DISCUSSION OF THE PHONON LASER SPECTRUM

1. Derivation of a free-run phonon laser linewidth

For a coherent oscillator, its spectrum linewidth is mainly dependent on the oscillator's phase noise. To simplify the process to obtain the phonon laser's linewidth, we only consider the influence of the phase noise.

For a harmonic oscillator at time t_0, its position and velocity can be written as

$$\begin{aligned} x_0 &= A_0 \sin(\Omega_0 t_0 + \varphi_0) \\ v_0 &= A_0 \Omega_0 \cos(\Omega_0 t_0 + \varphi_0). \end{aligned} \tag{D1}$$

Assuming at $t = t_0 + dt$ the oscillator obtains a stochastic impulse that changes its velocity to $v_0 + dv$, amplitude to $A_0 + dA$, phase to $\varphi_0 + d\varphi$, and x_0 unchanged, we then have

$$\begin{aligned} x_0 &= (A_0 + dA)\sin(\Omega_0 t_0 + \varphi_0 + d\varphi) \\ v_0 + dv &= (A_0 + dA)\Omega_0 \cos(\Omega_0 t_0 + \varphi_0 + d\varphi). \end{aligned} \tag{D2}$$

Expand out the trigonometric functions in Eq. (D2) and substitute Eq. (D1) into it. We have

$$\begin{aligned} x_0 &= \left(1 + \frac{dA}{A_0}\right)\left(x_0 \cos d\varphi + \frac{v_0}{\Omega_0}\sin d\varphi\right) \\ v_0 + dv &= \left(1 + \frac{dA}{A_0}\right)(v_0 \cos d\varphi - \Omega_0 x_0 \sin d\varphi). \end{aligned} \tag{D3}$$

Make a first-order approximation to trigonometric functions in Eq. (D3) and ignore $dAd\varphi$. We can solve Eq. (D3) to obtain

$$\begin{aligned} d\varphi &= -\frac{\Omega_0 x_0}{v_0^2 + \Omega_0^2 x_0^2} dv \\ &= -\frac{1}{\Omega_0 A_0}\sin(\Omega_0 t_0 + \varphi_0) dv. \end{aligned} \tag{D4}$$

As the stochastic force that induces the impulse can be written as $F_{\text{random}}(t) = \sqrt{2m\Gamma_0 k_B T_0}\,\xi(t)$, and $dv = F_{\text{random}}(t)dt/m$, $d\varphi$ can be written as

$$d\varphi = -\frac{1}{\Omega_0 A_0}\sqrt{\frac{2k_B T \Gamma_0}{m}}\sin(\Omega_0 t + \varphi) dW. \tag{D5}$$

Integrate the phase varying $\Delta\varphi$ in one oscillation period $\tau_0 = 2\pi/\Omega_0$. We have

$$\begin{aligned} \Delta\varphi &= -\frac{1}{\Omega_0 A_0}\sqrt{\frac{2k_B T \Gamma_0}{m}}\int_0^{\tau_0}\sin(\Omega_0 t + \varphi) dW \\ &= \frac{1}{\Omega_0 A_0}\sqrt{\frac{2k_B T \Gamma_0}{m}}\sqrt{\frac{1}{2}}W(\tau_0). \end{aligned} \tag{D6}$$

As the coherent time of the oscillator is much longer than τ_0, using quasistatic approximations and rewriting Eq. (D6) into a differentiated form, we have

$$d\varphi = \frac{1}{\Omega_0 A_0}\sqrt{\frac{k_B T \Gamma_0}{m}} dW. \tag{D7}$$

Next we focus on the oscillator trajectory autocorrelation. For a phonon laser, ignoring the amplitude fluctuation, its trajectory can be written as

$$x(t) = A_0 \cdot \sin[\Omega_0 t + \varphi(t)]. \tag{D8}$$

Its autocorrelation can be written as

$$R_{xx}(\tau) = \lim_{T\to\infty}\frac{1}{T}\int_{-T/2}^{T/2} x(t+\tau)x(t)dt. \tag{D9}$$

Try to solve the Eq. (D9). We have

$$\begin{aligned} R_{xx}(\tau) &= \frac{A_0^2}{2}\lim_{T\to\infty}\frac{1}{T}\int_{-T/2}^{T/2}\{\cos[\Omega_0\tau + \varphi(t+\tau) - \varphi(t)]dt - \cos[2\Omega_0 t + \Omega_0\tau + \varphi(t+\tau) + \varphi(t)]dt\} \\ &= \frac{A_0^2}{2}\lim_{T\to\infty}\frac{1}{T}\int_{-T/2}^{T/2}\cos[\Omega_0\tau + \varphi(t+\tau) - \varphi(t)]dt \\ &= \frac{A_0^2}{2}\cos(\Omega_0\tau)\lim_{T\to\infty}\frac{1}{T}\int_{-T/2}^{T/2}\cos[\varphi(t+\tau) - \varphi(t)]dt - \frac{A_0^2}{2}\sin(\Omega_0\tau)\lim_{T\to\infty}\frac{1}{T}\int_{-T/2}^{T/2}\sin[\varphi(t+\tau) - \varphi(t)]dt. \end{aligned} \tag{D10}$$

According to Eq. (D7),

$$\begin{aligned} R_{xx}(\tau) &= \frac{A_0^2}{2}\cos(\Omega_0\tau)\lim_{T\to\infty}\frac{1}{T}\int_{-T/2}^{T/2}\cos\left[\frac{1}{\Omega_0 A_0}\sqrt{\frac{k_B T\Gamma_0}{m}}W(\tau)\right]dt - \frac{A_0^2}{2}\sin(\Omega_0\tau)\lim_{T\to\infty}\frac{1}{T}\int_{-T/2}^{T/2}\sin\left[\frac{1}{\Omega_0 A_0}\sqrt{\frac{k_B T\Gamma_0}{m}}W(\tau)\right]dt \\ &= \frac{A_0^2}{2}\cos(\Omega_0\tau)\exp(-Dt), \end{aligned} \tag{D11}$$

where $D = k_B T_0 \Gamma_0/(2m\Omega_0^2 A_0^2)$ is the diffusion coefficient.

With the mean phonon number $\langle N\rangle$, we have $A_0 = \sqrt{2\langle N\rangle\hbar/(m\Omega_0)}$ and $D = k_B T_0\Gamma_0/(4\langle N\rangle\hbar\Omega_0)$.

To obtain the power spectrum density (PSD), the Wiener-Khinchin theorem is used in the Fourier transform of the autocorrelation R_{xx}. We have

$$S(\omega) = \frac{A_0^2 D\left(D^2 + \Omega_0^2 + \omega^2\right)}{(D^2 + \omega^2)^2 + 2(D^2 - \omega^2)\Omega_0^2 + \Omega_0^4}. \tag{D12}$$

Using two approximation conditions, which are $\Omega_0 \gg D$ and $\omega \simeq \Omega_0$, Eq. (D12) can be simplified to

$$S(\omega) = \frac{A_0^2}{2}\frac{D}{D^2 + (\omega - \Omega_0)^2}. \tag{D13}$$

Equation (D13) is a Lorentzian function. It has a linewidth that reads

$$\Delta\omega_{\text{FWHM}} = 2D = \frac{k_B T_0 \Gamma_0}{2\langle N\rangle\hbar\Omega_0}, \tag{D14}$$

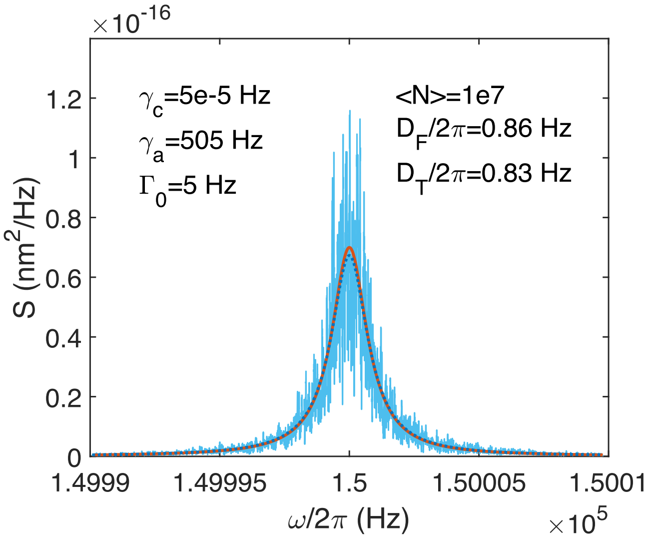

FIG. 8. Simulation of the free-run phonon laser spectrum. The blue line is the PSD of a simulated free-run phonon trajectory. The solid line is the theoretical PSD according to Eq. (D13). The dashed line is a Lorentz fitting of the simulation PSD. D_T is the theoretical diffusion coefficient. D_F is the fitted diffusion coefficient. The simulation condition is $\gamma_c = 5 \times 10^{-5}$ Hz, $\gamma_a = 505$ Hz, $\Gamma_0 = 5$ Hz, and $T_0 = 298$ K. The length of the simulation time is 500 s.

or

$$\Delta f_\mathrm{FWHM} = \frac{2D}{2\pi} = \frac{k_\mathrm{B} T_0 \Gamma_0}{4\pi \langle N \rangle \hbar \Omega_0}. \tag{D15}$$

The simulation result of the free-run phonon laser spectrum is shown in Fig. 8. The simulated PSD well matches the theoretical PSD in Eq. (D13).

2. Duffing nonlinearity-induced linewidth widening

However, due to the Duffing nonlinearity, it is difficult to experimentally obtain a free-run phonon laser with a PSD in Eq. (D13). As the optical potential along the trapping position is a Gaussian distribution, when the oscillator's amplitude is large, the oscillator's restoring force is in a Duffing nonlinear form, which is $F = k(x + \xi x^3)$, where $\xi = -2/w^2$ and w is the $1/e^2$ beam intensity radius at the trapping point. One of the effects of the nonlinearity is that there will be a frequency shift with different oscillation amplitudes, which is $\Delta\Omega = -\frac{3}{4} A_0^2 \Omega_0 / w^2$. Rewriting the frequency shift in phonon number form yields

$$\Delta\Omega = -\frac{3\hbar N}{2mw^2}. \tag{D16}$$

According to the phonon number distribution [Eq. (6) in the main text] of a phonon laser, the nonlinearity-induced frequency shift also has a distribution, which is

$$\rho(\Delta\Omega) = \frac{1}{Z_\Omega} \exp\left\{-\beta_0 \left(\frac{\hbar\Omega_0\gamma_c}{2\Gamma_0}\left[-\frac{2mw^2}{3\hbar}\Delta\Omega - \frac{(\gamma_a - \Gamma_0)}{\gamma_c}\right]^2\right)\right\}. \tag{D17}$$

Assume that the base frequency is a single frequency oscillation with a constant amplitude. The height of the spectrum at $\Omega_0 + \Delta\Omega'$ is proportional to $\rho(\Delta\Omega')$. The nonlinear-frequency-shift–induced spectrum width can be obtained by solving the two roots of $\rho(\Delta\Omega_{\mathrm{half\_max1(2)}}) = 1/2Z_\Omega$. And $\Delta\Omega_\mathrm{FWHM} = |\Delta\Omega_{\mathrm{half\_max1}} - \Delta\Omega_{\mathrm{half\_max2}}|$, which is

$$\Delta\Omega_\mathrm{FWHM} = \frac{3\hbar}{mw^2}\sqrt{(\ln 2)\frac{2\Gamma_0}{\beta_0\hbar\Omega_0\gamma_c}}. \tag{D18}$$

Or write with the standard deviation of phonon number $\sigma_N = \sqrt{k_\mathrm{B} T_0 \Gamma_0 / \hbar\Omega_0\gamma_c}$, which is

$$\Delta\Omega_\mathrm{FWHM} = \frac{3\hbar}{mw^2}\sigma_N\sqrt{2\ln 2}. \tag{D19}$$

With the same simulation conditions shown in Fig. 8 and $w = 550$ nm, $m = 3 \times 10^{-18}$ kg, we have the nonlinearity-induced width is $\Delta\Omega_\mathrm{FWHM} = 2\pi \times 187.9$ Hz, which is much larger than the phase-noise-induced width of $\Delta\omega_\mathrm{FWHM} = 2D_\mathrm{T} = 2\pi \times 1.6$ Hz.

---

[1] J. M. R. Parrondo, J. M. Horowitz, and T. Sagawa, Thermodynamics of information, Nat. Phys. **11**, 131 (2015).
[2] E. Lutz and S. Ciliberto, Information: From Maxwell's demon to Landauer's eraser, Phys. Today **68**(9), 30 (2015).
[3] U. Seifert, Stochastic thermodynamics, fluctuation theorems and molecular machines, Rep. Prog. Phys. **75**, 126001 (2012).
[4] F. S. Gnesotto, F. Mura, J. Gladrow, and C. P. Broedersz, Broken detailed balance and non-equilibrium dynamics in living systems: A review, Rep. Prog. Phys. **81**, 066601 (2018).
[5] S. Amano, M. Esposito, E. Kreidt, D. A. Leigh, E. Penocchio, and B. M. W. Roberts, Insights from an information thermodynamics analysis of a synthetic molecular motor, Nat. Chem. **14**, 530 (2022).
[6] L. Rondin, J. Gieseler, F. Ricci, R. Quidant, C. Dellago, and L. Novotny, Direct measurement of Kramers turnover with a levitated nanoparticle, Nat. Nanotechnol. **12**, 1130 (2017).
[7] M. Rashid, T. Tufarelli, J. Bateman, J. Vovrosh, D. Hempston, M. S. Kim, and H. Ulbricht, Experimental Realization of a Thermal Squeezed State of Levitated Optomechanics, Phys. Rev. Lett. **117**, 273601 (2016).
[8] A. Militaru, M. Innerbichler, M. Frimmer, F. Tebbenjohanns, L. Novotny, and C. Dellago, Escape dynamics of active particles in multistable potentials, Nat. Commun. **12**, 2446 (2021).
[9] U. Delić, M. Reisenbauer, K. Dare, D. Grass, V. Vuleti, N. Kiesel, and M. Aspelmeyer, Cooling of a levitated nanoparticle to the motional quantum ground state, Science **367**, 892 (2020).
[10] F. Tebbenjohanns, M. L. Mattana, M. Rossi, M. Frimmer, and L. Novotny, Quantum control of a nanoparticle optically levitated in cryogenic free space, Nature (London) **595**, 378 (2021).
[11] L. Magrini, P. Rosenzweig, C. Bach, A. Deutschmann-Olek, S. G. Hofer, S. Hong, N. Kiesel, A. Kugi, and M. Aspelmeyer,

Real-time optimal quantum control of mechanical motion at room temperature, Nature (London) **595**, 373 (2021).

[12] J. Ahn, Z. Xu, J. Bang, P. Ju, X. Gao, and T. Li, Ultrasensitive torque detection with an optically levitated nanorotor, Nat. Nanotechnol. **15**, 89 (2020).

[13] F. Ricci, M. T. Cuairan, G. P. Conangla, A. W. Schell, and R. Quidant, Accurate mass measurement of a levitated nanomechanical resonator for precision force-sensing, Nano Lett. **19**, 6711 (2019).

[14] F. Monteiro, S. Ghosh, A. G. Fine, and D. C. Moore, Optical levitation of 10-ng spheres with nano-g acceleration sensitivity, Phys. Rev. A **96**, 063841 (2017).

[15] D. Hempston, J. Vovrosh, M. Toroš, G. Winstone, M. Rashid, and H. Ulbricht, Force sensing with an optically levitated charged nanoparticle, Appl. Phys. Lett. **111**, 133111 (2017).

[16] B. Rodenburg, L. P. Neukirch, A. N. Vamivakas, and M. Bhattacharya, Quantum model of cooling and force sensing with an optically trapped nanoparticle, Optica **3**, 318 (2016).

[17] T. Li, S. Kheifets, D. Medellin, and M. G. Raizen, Measurement of the instantaneous velocity of a Brownian particle, Science **328**, 1673 (2010).

[18] J. Gieseler, R. Quidant, C. Dellago, and L. Novotny, Dynamic relaxation of a levitated nanoparticle from a non-equilibrium steady state, Nat. Nanotechnol. **9**, 358 (2014).

[19] J. Gieseler, L. Novotny, C. Moritz, and C. Dellago, Non-equilibrium steady state of a driven levitated particle with feedback cooling, New J. Phys. **17**, 045011 (2015).

[20] M. Debiossac, D. Grass, J. J. Alonso, E. Lutz, and N. Kiesel, Thermodynamics of continuous non-Markovian feedback control, Nat. Commun. **11**, 1360 (2020).

[21] A. Militaru, A. Lasanta, M. Frimmer, L. L. Bonilla, L. Novotny, and R. A. Rica, Kovacs Memory Effect with an Optically Levitated Nanoparticle, Phys. Rev. Lett. **127**, 130603 (2021).

[22] J. Gieseler and J. Millen, Levitated nanoparticles for microscopic thermodynamics: A review, Entropy **20**, 326 (2018).

[23] J. Sheng, C. Yang, and H. Wu, Nonequilibrium thermodynamics in cavity optomechanics, Fundam. Res. **3**, 75 (2022).

[24] R. M. Pettit, W. Ge, P. Kumar, D. R. Luntz-Martin, J. T. Schultz, L. P. Neukirch, M. Bhattacharya, and N. A. Vamivakas, An optical tweezer phonon laser, Nat. Photon. **13**, 402 (2019).

[25] J. Gieseler, B. Deutsch, R. Quidant, and L. Novotny, Subkelvin Parametric Feedback Cooling of a Laser-Trapped Nanoparticle, Phys. Rev. Lett. **109**, 103603 (2012).

[26] Y. Zheng, L.-M. Zhou, Y. Dong, C.-W. Qiu, X.-D. Chen, G.-C. Guo, and F.-W. Sun, Robust Optical-Levitation-Based Metrology of Nanoparticle's Position and Mass, Phys. Rev. Lett. **124**, 223603 (2020).

[27] Y. Zheng, G.-C. Guo, and F.-W. Sun, Cooling of a levitated nanoparticle with digital parametric feedback, Appl. Phys. Lett. **115**, 101105 (2019).

[28] A. Bérut, A. Arakelyan, A. Petrosyan, S. Ciliberto, R. Dillenschneider, and E. Lutz, Experimental verification of Landauer's principle linking information and thermodynamics, Nature (London) **483**, 187 (2012).

[29] K. Vahala, M. Herrmann, S. Knünz, V. Batteiger, G. Saathoff, T. W. Hänsch, and T. Udem, A phonon laser, Nat. Phys. **5**, 682 (2009).

[30] I. S. Grudinin, H. Lee, O. Painter, and K. J. Vahala, Phonon Laser Action in a Tunable Two-Level System, Phys. Rev. Lett. **104**, 083901 (2010).

[31] J. Zhang, B. Peng, Ş. K. Özdemir, K. Pichler, D. O. Krimer, G. Zhao, F. Nori, Y.-X. Liu, S. Rotter, and L. Yang, A phonon laser operating at an exceptional point, Nat. Photon. **12**, 479 (2018).

[32] Z. Liu, Y. Wei, L. Chen, J. Li, S. Dai, F. Zhou, and M. Feng, Phonon-Laser Ultrasensitive Force Sensor, Phys. Rev. Appl. **16**, 044007 (2021).

[33] J. Gieseler, L. Novotny, and R. Quidant, Thermal nonlinearities in a nanomechanical oscillator, Nat. Phys. **9**, 806 (2013).

[34] J. Gieseler, M. Spasenovic, L. Novotny, and R. Quidant, Nonlinear Mode Coupling and Synchronization of a Vacuum-Trapped Nanoparticle, Phys. Rev. Lett. **112**, 103603 (2014).

[35] J. Flajšmanová, M. Šiler, P. Jedlička, F. Hrubý, O. Brzobohatý, R. Filip, and P. Zemánek, Using the transient trajectories of an optically levitated nanoparticle to characterize a stochastic duffing oscillator, Sci. Rep. **10**, 14436 (2020).

[36] T. Westphal, H. Hepach, J. Pfaff, and M. Aspelmeyer, Measurement of gravitational coupling between millimetre-sized masses, Nature (London) **591**, 225 (2021).

[37] K. Proesmans, J. Ehrich, and J. Bechhoefer, Finite-Time Landauer Principle, Phys. Rev. Lett. **125**, 100602 (2020).

[38] R. D. Astumian, Thermodynamics and kinetics of a Brownian motor, Science **276**, 917 (1997).

[39] J. Bang, R. Pan, T. M. Hoang, J. Ahn, C. Jarzynski, H. T. Quan, and T. Li, Experimental realization of Feynman's ratchet, New J. Phys. **20**, 103032 (2018).

[40] Z. Lu and O. Raz, Nonequilibrium thermodynamics of the Markovian Mpemba effect and its inverse, Proc. Natl. Acad. Sci. USA **114**, 5083 (2017).

[41] A. Kumar and J. Bechhoefer, Exponentially faster cooling in a colloidal system, Nature (London) **584**, 64 (2020).

[42] Y. Arita, S. H. Simpson, P. Zemánek, and K. Dholakia, Coherent oscillations of a levitated birefringent microsphere in vacuum driven by nonconservative rotation-translation coupling, Sci. Adv. **6**, eaaz9858 (2020).